Oxidation of propane to acrylic acid over vanadyl pyrophosphate: modifications of the structural and acid properties during the precursor activation and their relationship with catalytic performances

G. Landi[a,*], L. Lisi[b], J.-C. Volta[c]

[a] *Dip. di Ing. Chimica, University of Napoli Federico II, P.le Tecchio 80, 80125 Napoli, Italy*
[b] *Istituto di Ricerche sulla Combustione, CNR, P.le Tecchio 80, 80125 Napoli, Italy*
[c] *Institut des Recherches sur la Catalyse, CNRS, 2 Av. Einstein, 69626 Villeurbanne, France*

Abstract

The modifications of vanadyl pyrophosphate (VPO) during the activation under propane/oxygen/water/nitrogen containing gaseous mixture have been studied and related to catalytic performances of the catalyst in the oxidation of propane to acrylic acid (AA). VPO samples activated at different times starting from $VOHPO_4 \cdot 0.5H_2O$ have been characterized by using SEM, XRD, ^{31}P NMR by spin echo mapping and NH_3-TPD techniques. Introduction of water after about 20 h results in enhancing crystallization of the catalyst, reducing surface acidity (also changing acid sites distribution) and promoting the disappearance of V^{5+}-containing phases. At the same time, acrylic acid is produced and its selectivity is improved up to 40 h activation of the catalyst. Stable catalytic performances and physico-chemical properties are then observed.
© 2004 Elsevier B.V. All rights reserved.

Keywords: Propane mild oxidation; Acrylic acid; Vanadyl pyrophosphate; Crystallinity; Surface acidity; V^{+5} phases

1. Introduction

Alkanes can be used to obtain fine chemicals through selective oxidation processes [1]; these could be developed on the basis of heterogeneous catalysed reactions either with the simultaneous presence of the alkane and molecular oxygen or by separating the reduction stage, in which the product is obtained at the expense of the oxygen of the catalyst, from the oxidizing stage during which the catalyst is re-oxidized in oxygen-rich streams. Examples can be found on vanadyl pyrophosphate (VPO) catalysts for the production of maleic anhydride from *n*-butane [2–5]. The most important advantages for substituting alkanes to alkenes and aromatics for the production of fine chemicals are the one-stage process, the lower cost and the reduced environ-

mental impact. Nevertheless, the low selectivity of partial oxidation reactions of alkanes makes such processes not yet profitable.

The selective oxidation of propane appears promising for the production of propylene, oxygenates (acrolein and acrylic acid (AA)) and acrylonitrile [6–21]. Particularly, a great effort has been done to modify the catalyst formulation and the preparation method in order to enhance the selectivity for the desired product.

VPO-based catalysts are claimed among those active for production of AA; up to now, modifications of the catalyst composition [6,8,10–12,22,23] have been attempted to enhance the low VPO selectivity to AA, with quite limited successes. On the contrary, the modification of the gas phase composition, particularly the water vapour concentration [6,12,24,25], showed a more significant influence on AA yield both during the reaction and the activation of the hemihydrate precursor. Nevertheless, it is not well understood

---

* Corresponding author. Tel.: +39 0817682233; fax: +39 0815936936.
E-mail address: landi@unina.it (G. Landi).

which properties of the catalyst are involved and modified in the selective oxidation of propane. Several papers have been published on the characterization of VPO under *n*-butane/oxygen gas mixture and for different preparations in order to match structural and surface modifications and catalytic performances [26–41], but less attention has been paid to the effect of propane/oxygen mixture on the activation of VPO. Features, like crystallinity, V^{5+}-containing phases (amount and type) and acidity (amount and type), appear related to activity and selectivity to maleic anhydride. From literature some considerations can be pointed out: as concerns crystallinity, disorganization of VPO is related to higher redox capacity and to better catalytic performances [26,27]. Recently, Duarte et al. [28] demonstrated that increasing surface defects corresponds to an increase of hydrocarbon activation. However, it must be underlined that a completely amorphous catalysts is not able to produce maleic anhydride, as reported by Abon et al. [29].

As concerns V^{5+}-containing phases, it is generally accepted that a little amount of $VOPO_4$, dispersed in the VPO matrix, is necessary to achieve a good selectivity to maleic anhydride [26–34]. It has been proposed that the amount of these phases (generally α_{II} or δ), generated during the activation procedure [26], are related to the selectivity to maleic anhydride. On the contrary, some authors [35,36] did not detect any phase different from pure vanadyl pyrophosphate, while Cavani et al. [37] recently proposed that V^{3+} sites are involved in the selective reaction pathway.

Also surface acidity (type and distribution of sites) is related to activity and selectivity to maleic anhydride [28,38–41]. Lewis acid sites have been considered as activating sites for *n*-C_4 [40], while higher selectivity to maleic anhydride has been associated to the increase of the Brønsted acidity [28,39].

The aim of this work is to elucidate which VPO features are involved in propane mild oxidation studying the evolution of the material with time-on-stream during the activation and to underline similitudes and differences with *n*-butane mild oxidation.

2. Experimental

2.1. Preparation of precursor

VPO catalyst was prepared by Exxon organic method [12], adding V_2O_5 (11.8 g) and H_3PO_4 (9.7 cm^3, 85%) to isobutanol (250 cm^3). This mixture was heated up to isobutanol boiling point (105 °C) and then refluxed for 16 h under an inert atmosphere (N_2). A condensator provides recovering of isobutanol vapours in order to keep the suspension volume constant. After 16 h refluxing, the suspension is light blue; the solid is separated from the liquid by filtration and washed with isobutanol and ethanol. The resulting solid is refluxed in hot water (9 cm^3 H_2O/g_{solid}), filtered and dried in air at 110 °C for 16 h. The vanadyl acid phosphate hemihydrate

($VOHPO_4 \cdot 0.5H_2O$) obtained is the precursor of vanadyl pyrophosphate.

2.2. Catalyst activation

Activation was carried out to transform the precursor into the active catalyst, according to the procedure reported elsewhere [24]. Precursor was placed in a fixed-bed microreactor under a gas flow mixture ($W/F = 0.4$ (g h)/dm^3) containing propane, oxygen and nitrogen (1.6/17.8/80.6 vol.%) and heated up to 430 °C. After 17 h the temperature was lowered down to 400 °C and 2.5 h later water vapour was introduced in the mixture ($C_3H_8/O_2/H_2O/N_2 = 1.6/17.8/20/60.6$ vol.%), without changing the total flow rate. This study has been carried out on samples activated 17 (V1), 28 (V2), 42 (V3), 64 (V4) and 90 h (V5), respectively.

2.3. Characterization techniques

Chemical composition of VPO precursor was determined by atomic emission spectroscopy with an ICP spectro-flame (inducting coupling plasma) from Spectro after dissolution of the solid in hydrochloric acid.

2.3.1. SEM
Scanning electron microscopy was performed with a Philips XL 30 microscope. Enlargements between 5000× and 30,000× have been used to better define typical morphological structures of the samples.

2.3.2. XRD diffraction
XRD was performed with a Siemens D500 diffractometer using Cu Kα at 35 kV and 30 mA. Parameters, like peak intensity and full-with at half-maximum (FWHM), have been calculated using a dedicated software (DiffractoPlus Eva).

2.3.3. BET measurements
BET surface areas were measured by N_2 adsorption at 77 K with a 1900 Carlo Erba Sorptomatic.

2.3.4. ^{31}P NMR
^{31}P NMR spin-echo mapping spectra have been recorded on a Bruker MSL 300 NMR spectrometer, under static conditions, using a $90°x$–τ–$180°y$–τ-acquire sequence. The $90°$ pulse was 4.2 μs and τ was 20 μs. For each sample, the irradiation frequency was varied in increments of 50 kHz above and below the ^{31}P resonance of H_3PO_4. The number of spectra thus recorded was dictated by the frequency limits beyond which no spectral intensity was visible. The ^{31}P NMR spin-echo mapping information was then obtained by superposition of all spectra.

2.3.5. Temperature programmed desorption of ammonia (NH$_3$-TPD)
Temperature programmed desorption of ammonia (NH$_3$-TPD) was performed using a Micromeretics TPD/TPR 2900

analyser equipped with a TC detector and coupled with a Hiden HPR 20 mass spectrometer. After a pre-treatment at 200 °C under helium flow, to desorb the physisorbed water, the sample was saturated with ammonia at 100 °C. After purging at 100 °C, NH_3 was desorbed heating at constant rate (10 °C/min) up to 620 °C. Masses of ammonia and other products, possibly produced or desorbed during the experiment, like water, nitrogen and its oxides were followed with the mass spectrometer. In our experiments only ammonia was detected. In order to separate contributions of different acid sites, deconvolution of TPD peaks has been performed using a dedicated software, supposing curves had a Gaussian-type shape and that each signal was composed by three peaks which correspond to the minimum number to obtain a good superposition of experimental and calculated signal.

3. Results

3.1. Characterization of materials

Chemical analysis showed that the phosphorus/vanadium ratio of the VPO precursor is around one, in agreement with the elemental formula of the vanadyl acid phosphate hemihydrate $VOHPO_4 \cdot 0.5H_2O$.

3.2. SEM

In Fig. 1, a SEM image of the VPO precursor, labelled P, showing the typical lamellar rose-like structure, is reported. SEM micrographs of the activated samples are labelled according to the nomenclature reported in the experimental section. Results of SEM analysis revealed that the V1
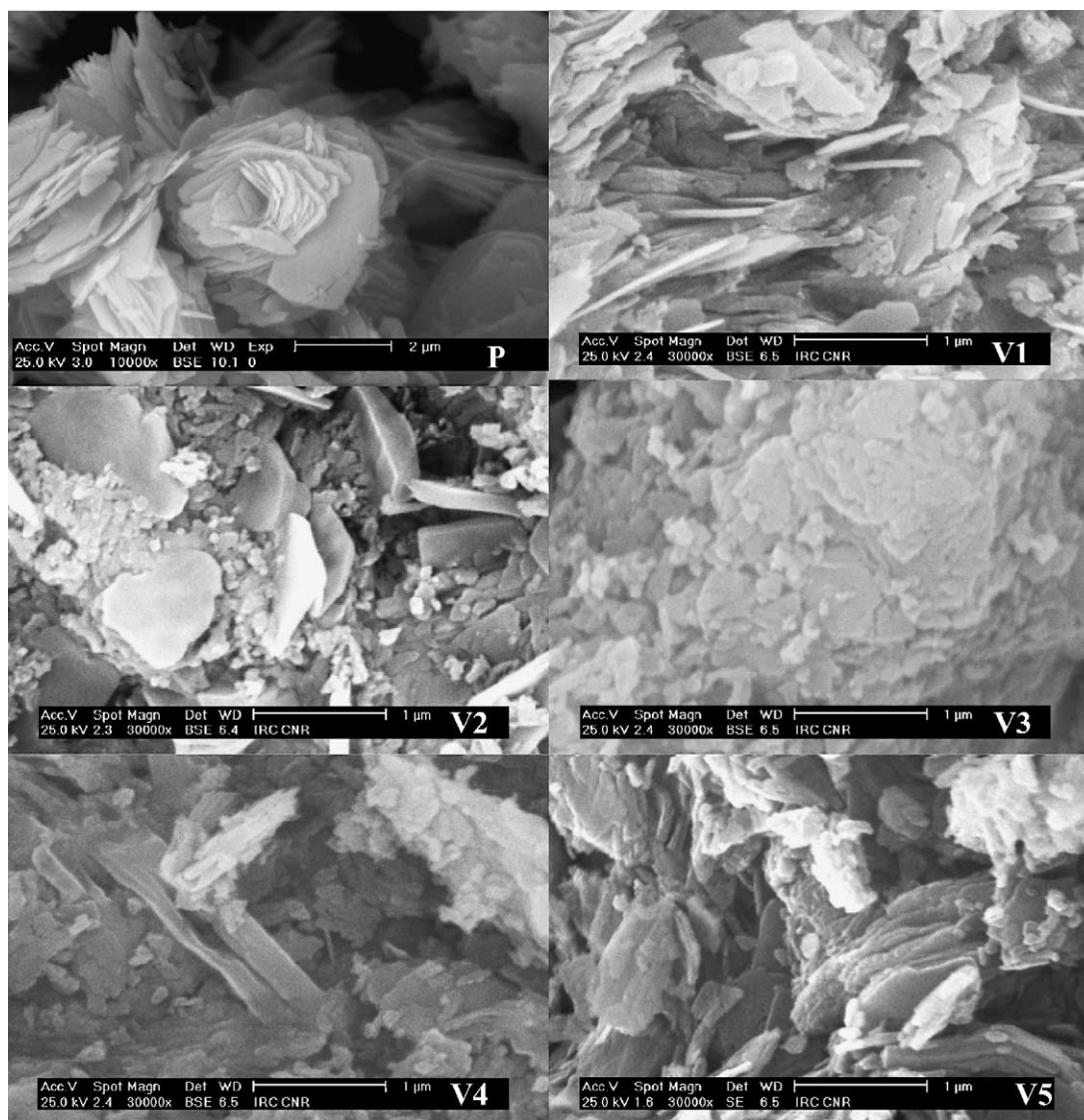

Fig. 1. SEM images of precursor (P) and samples activated for different times: V1 (17 h), V2 (28 h), V3 (42 h), V4 (64 h) and V5 (90 h).
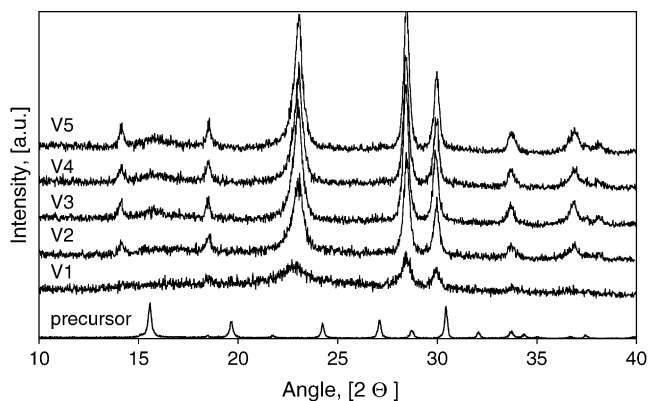
Fig. 2. XRD spectra of VPO precursor (P) and activated samples.

Fig. 3. FWHM values of XRD peaks of principal planes on activated samples.

sample is mainly constituted of small lamellae as the precursor but the rose-like structure is partially lost and a preferential orientation of lamellae is observed. With the time-on-stream and upon water introduction, the morphological structure changes, due to overlapping and growth of lamellae.

3.3. XRD diffraction

As shown in Fig. 2, the XRD spectrum of the precursor is typical of well-crystallized vanadyl acid phosphate hemihydrate: intense and narrow peaks appear at about $15.6°$ and $30.4°$, corresponding to the main planes $((0\,0\,1)$ and $(2\,2\,0)$, respectively). XRD spectra of the VPO samples corresponding to different times of activation are reported in the same figure. In order to avoid superposition among the different spectra in Fig. 2, XRD pattern of the precursor has been scaled by a factor 10. Vanadyl pyrophosphate $(VO)_2P_2O_7$ is the only phase detected for activated samples, suggesting that transformation from $VOHPO_4 \cdot 0.5H_2O$ into vanadyl pyrophosphate already occurs during the first step in the absence of water. Crystallinity increases with time-on-stream, particularly during the first 40 h (samples V1–V3) as shown by the decrease of the FWHM values of the $(2\,0\,0)$, $(0\,2\,4)$ and $(0\,3\,2)$ signals at $23°$, $28.4°$ and $29.9°$, respectively, and the increase of intensity of the corresponding lines. The most marked development is that of the $(2\,0\,0)$ plane, FWHM of the corresponding signal being reduced from about $1°$ to $0.45°$ (see Fig. 3). Accordingly, the intensity of the peak shows the highest increase. As already mentioned, the structural modifications are more evident in the first 40 h, only a slight increase of peak intensity having been observed in the last three samples (samples V3–V5).

3.4. BET measurements

BET surface areas were all in the range 8–12 m²/g, as expected for these materials [26,29,41].

3.5. ^{31}P NMR
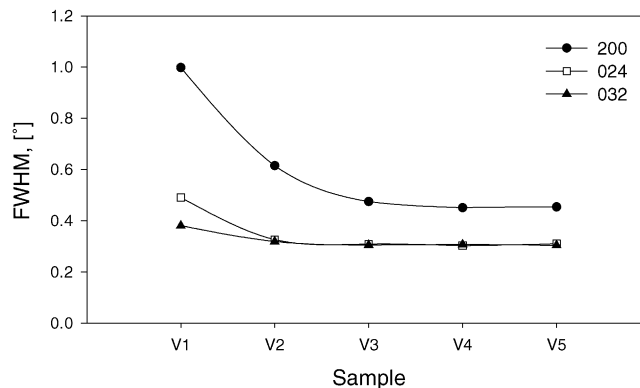
^{31}P NMR by spin echo mapping have been performed in order to detect any V^{3+}- and/or V^{5+}-containing phase, not detectable by X-Ray diffraction. This technique is a powerful tool to discern different vanadium phosphate phases, as shown by Tuel et al. [42]. Spectrum recorded on precursor, reported in Fig. 4, shows only the signal of the vanadyl acid phosphate hemihydrate at about 1750 ppm, in agreement with the XRD results, confirming that $VOHPO_4 \cdot 0.5H_2O$ is the only phase constituting the precursor. The ^{31}P NMR spin echo mapping spectra registered on the activated samples are also reported in Fig. 4. The first sample, V1, shows a significant signal at 0 ppm due to V^{5+}-containing phases, not detectable by XRD, and the signal of V^{4+} at around 2600 ppm characteristic of P atoms connected to V^{4+} in the $(VO)_2P_2O_7$ structure [42]. The contribution of V^{5+}-containing phases decreases for V2 sample, i.e. after water introduction. For the other samples, V3, V4 and V5, only signals characteristic of vanadyl pyrophosphate are observed. The peak maximum of vanadyl pyrophosphate at 2600 ppm slightly shifts to higher
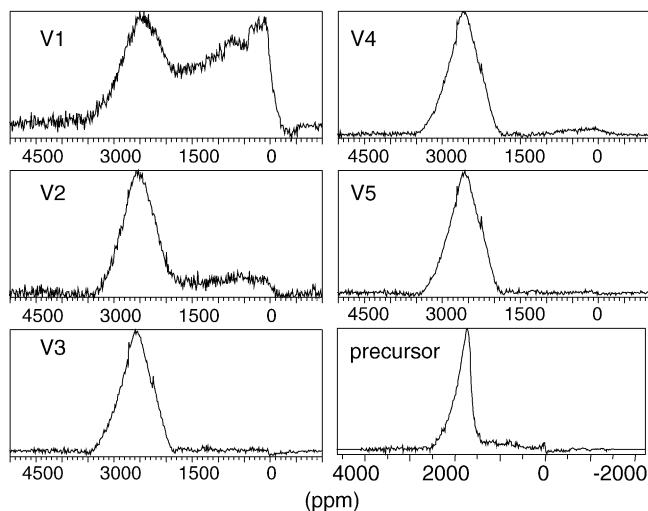

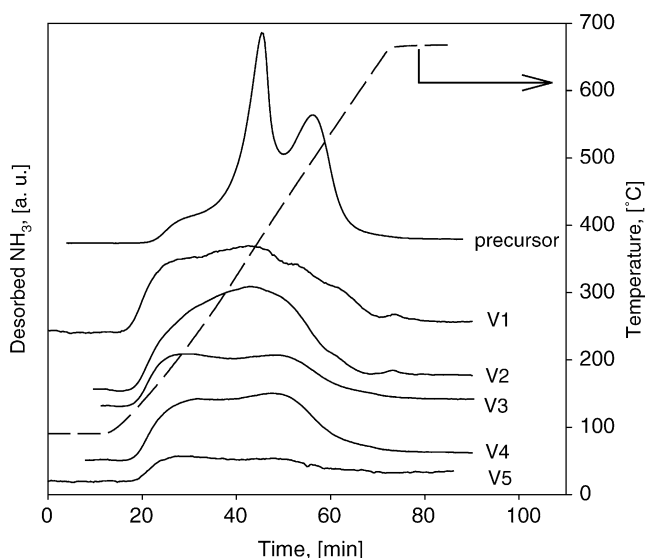Fig. 4. ^{31}P NMR spectra of VPO precursor and activated samples.

Fig. 5. NH$_3$-TPD profiles of VPO precursor and activated samples.

frequencies for samples V1–V3, indicating that crystallization of $(VO)_2P_2O_7$ is occurring. No further shifts have been observed in the spectra of samples V4 and V5.

3.6. NH$_3$-TPD

The surface acidity of the VPO precursor and of the catalysts has been measured by ammonia adsorption. Fig. 5 shows the desorption of ammonia measured during the TPD experiments. The total amount of ammonia desorbed during the TPD experiments, evaluated from the integration of curves, is reported in Fig. 6. Two quite well defined peaks, with maximum at 340 and 450 °C, respectively, and a shoulder at about 180 °C are recognizable for the NH$_3$-TPD of precursor. The amount of acid sites, very high for the precursor, decreases for the activated samples. This amount further decreases with time-on-stream among the activated materials (see Fig. 6). Different peaks, much more overlapped compared to those of the precursor, contribute to the whole TPD signal of activated samples. In order to evaluate the contribution of these
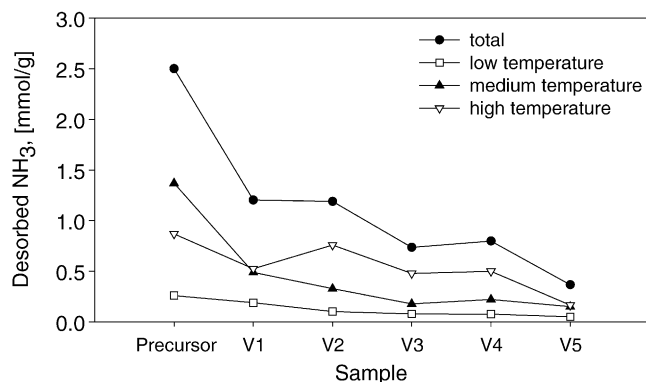
peaks, corresponding to different acid sites, a deconvolution of the TPD signals was performed using a peak fit software, as described in the Experimental section. The only constraint used was the number of peaks that was supposed three as for the precursor. The values of peak temperature of calculated signals are in a quite narrow window suggesting that the deconvolution procedure used allows the determination of peaks having the same nature for each catalyst. The first peak is located around 180 °C for all samples. The maximum temperature of the second peak of V1 sample is about 290 °C, while it decreases upon water introduction down to about 240 °C, suggesting a weakening of these sites or the addition of a component at lower temperature related to the presence of water. Likewise, the last signal, located at about 450 °C for the V1 sample, shifts at about 400 °C for the others. In conclusion, in addition to the strong change of acidity related to the transformation from precursor to pyrophosphate, modifications associated to the introduction of water in the activation mixture promoted the shift towards lower temperature of TPD peaks. As concerns the number of acid sites, a general decrease of acidity from precursor to V5 is observed, transformation from hemihydrate to pyrophosphate giving the largest loss. Areas of low and medium temperature peaks also decrease with activation time reaching a stable value after 40 h activation. On the contrary, area of high temperature peak does not uniformly decreases, showing a slight maximum for V2, a quite constant value for V3 and V4 and a further decrease for V5. As known, NH$_3$-TPD measurements do not give information about the type of the acidity. However, we can try to define the type of the acidity associated to each peak on the base of literature data. Brønsted acid sites of vanadyl pyrophosphate are stronger than Lewis ones; moreover, during pyridine desorption a slight maximum in Brønsted acid sites amount simultaneously to the decrease of Lewis acid sites has been found [28]. These features induce us to assign the high temperature peak to the Brønsted acidity. The other peaks could be assigned to two different Lewis acid sites.

3.7. Catalytic results

Fig. 7 shows catalytic performance of VPO as a function of the time-on-stream. Vertical lines indicate the final time of each experiment. During the first activation step, at 430 °C in the absence of water in the feed stream, the propane conversion was high and only products of combustion were detected. Low amounts of propylene and traces of ethane and ethylene were detected when temperature was lowered at 400 °C, while propane conversion decreased. As reported before [6,12,24], selectivity to acrylic acid increased significantly only after introducing water in the flow (20%); at the same time propane conversion further decreased whereas propylene, ethane and ethylene disappeared and a low amount of acetic acid was detected. The enhancement of AA selectivity was mainly balanced by the decrease of CO selectivity whereas production of CO$_2$ was almost unaffected by
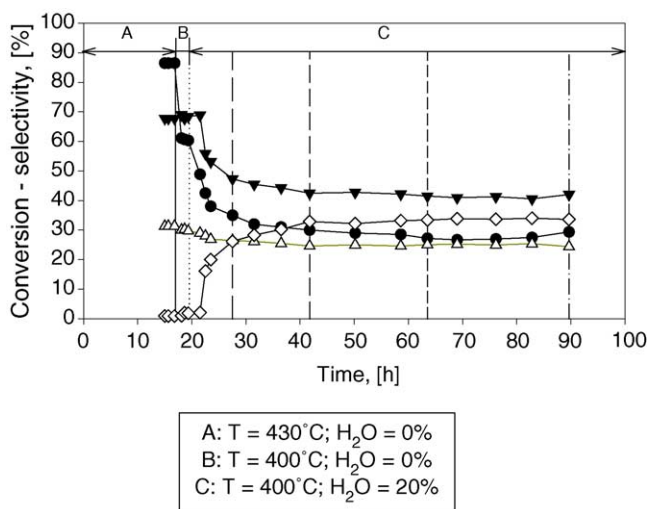

Fig. 6. Total and partial amounts of NH$_3$ desorbed during TPD experiments on VPO precursor and activated samples.

Fig. 7. Propane conversion ($\bullet$), selectivities to AA ($\diamond$), CO ($\blacktriangledown$) and CO$_2$ ($\triangle$) as a function of the time-on-stream during activation.

reaction conditions. After about 20 h under wet mixture, the catalytic performances of VPO became stable, since no significant changes were detected both for propane conversion and for products selectivity: final value of conversion was about 28% and selectivity to AA about 32%. Therefore, it can be assumed that an activation procedure interrupted after 20 h in water-containing mixture provides a catalytically stable sample.

4. Discussion

Both physico-chemical characterisation and catalytic activity indicate that the VPO catalyst significantly evolves during first 40 h activation. After this period, no further modifications of either structure and catalytic performances are detectable. Transformation from precursor into pyrophosphate occurs also in the absence of water, however, water introduction results into a significant increase of crystallization of the poorly crystallized material obtained in the absence of water. Crystallization degree is then slowly improved with time-on-stream up to a constant value after 40 h. At the same time disappearance of V^{5+} isolated sites and microdomains occurs suggesting that hemihydrate is transformed into pyrophosphate through formation of VOPO$_4$ regions as proposed by Abon et al. [29].

Structural reorganisation of the VPO material is also detectable through the modification of morphology as shown by the loss of the typical rose-like structure for a preferential orientation of lamellae promoted by the presence of water likely through the dissolution of the small fraction of water-soluble VOPO$_4$, as suggested by Xue and Schrader for VPO under *n*-butane/oxygen/water mixture [43]. The role of solubilized fraction can be then supposed to promote the slipping and the union of VPO lamellae to form larger pyrophosphate crystals.

As concerns surface, the strong acidity of the precursor is markedly reduced (both number and strength of acid sites) due to transformation into pyrophosphate. Moreover, a further loss of acidity is observed upon water introduction likely related to reorganisation of bulk structure. The modification of acid sites distribution between Brønsted and Lewis ones induces us to consider the last ones mainly involved in the AA formation.

By comparison of these results with catalytic performances, it can be concluded that, although the presence of water is necessary to produce acrylic acid, its selectivity increases with enhancing the order of crystalline structure and decreasing the surface acidity. Therefore, in contrast with results found for the oxidation of *n*-butane to maleic anhydride, formation of acrylic acid from propane requires a well-crystallised VPO catalyst with a low acidity suggesting that acid sites activating propane are also able to oxidise acrylic acid to CO$_x$.

Although, the role of crystalline structure is more difficult to be defined, the very slow response of the catalytic system to water introduction seems to confirm that the bulk structure is involved in the reaction of AA formation. In fact, AA is produced only after 5–6 h (Fig. 7) after water is fed to the reactor suggesting the occurrence of a deep modification of the material not limited to its surface, a faster process being expected in this latter case. The effect of bulk structure can be indirectly correlated to catalytic properties through a reduction of surface acidity or it can be related to a reduced oxygen availability in a well crystallised material inhibiting the further oxidation of the intermediate and/or the desired product.

Finally, the disappearance of V^{5+}-containing phases, claimed as active centres in the formation of maleic anhydride from *n*-butane, in the active and selective materials suggests that these phases are not involved in the selective pathway to acrylic acid. Moreover, this result demonstrates, in contrast with the *n*-butane oxidation to maleic anhydride, that the propane oxidation to acrylic acid is not associated to the isolation of V^{5+} sites, but is catalysed by a well-crystallised material with (VO)$_2$P$_2$O$_7$ structure.

5. Conclusions

Transformation of VOHPO$_4$·0.5H$_2$O into vanadyl pyrophosphate through an activation procedure under propane/oxygen/nitrogen mixture occurs during the first period (<17 h) of treatment at 430 °C in the absence of water. Nevertheless, a slow structural reorganisation of the bulk structure of the material occurs upon water introduction in the gas mixture, related to a slow modification of the catalytic properties. Increase of crystallinity, decrease of surface acidity and a progressive disappearance of V^{5+}-containing phases show the same trend of the improvement of acrylic acid selectivity. Forty hours of activation is sufficient to obtain a stable material with stable catalytic performances.

In conclusion, pure and well-crystallised vanadyl pyrophosphate with a low surface acidity is a good catalyst for the oxidation of propane to acrylic acid in contrast with the oxidation of *n*-butane to maleic anhydride requiring the presence of crystal defects and V^{5+}-containing domains to obtain the best performances.

Acknowledgments

References

[1] F. Cavani, F. Trifirò, Catal. Today 51 (1999) 561.
[2] R.M. Contractor, US Patent 4,668,802 (1987), to DuPont.
[3] G.D. Suciu, G. Stefani, C. Fumagalli, US Patent 4,511,670 (1985), to Lummus Crest Inc. and Alusuisse Italia SpA.
[4] H. Taheri, US Patent 5,011,945 (1991), to Amoco Co.
[5] G.K. Kwentus, M. Suda, US Patent 4,501,907 (1985), to Monsanto Co.
[6] M.M. Lin, Appl. Catal., A 207 (2001) 1.
[7] M.M. Bettahar, G. Costentin, L. Savary, J. Lavalley, Appl. Catal., A 145 (1996) 1.
[8] M. Ai, J. Catal. 101 (1986) 389.
[9] M. Ai, Catal. Today 13 (1992) 679.
[10] M. Ai, J. Mol. Catal. A: Chem. 114 (1996) 3.
[11] M. Ai, Catal. Today 42 (1998) 297.
[12] G. Landi, L. Lisi, J.-C. Volta, Chem. Commun. (2003) 492.
[13] B. Kerler, A.M.M.-M. Pohl, M. Baerns, Catal. Lett. 78 (2002) 259.
[14] X. Zhang, H.-l. Wan, W.-z. Weng, X.-d. Yi, J. Mol. Catal. A: Chem. 200 (2003) 291.
[15] J.N. Al-Saeedi, V.V. Guliants, O. Guerriero-Pérez, M.A. Bañares, J. Catal. 215 (2003) 108.
[16] J.M. Lopez Nieto, P. Rotella, B. Solsona, J.M. Oliver, Catal. Today 81 (2003) 87.
[17] S.H. Taylor, A.J.J. Pollard, Catal. Today 81 (2003) 179.
[18] P. Botella, J.M. Lopez Nieto, B. Solsona, A. Mifsud, F. Marquez, J. Catal. 209 (2002) 445.
[19] P. Viparelli, P. Ciambelli, L. Lisi, G. Ruoppolo, G. Russo, J.-C. Volta, Appl. Catal., A 184 (1999) 291.
[20] A.A. Lemonidou, L. Nalbandian, I.A. Vasalos, Catal. Today 61 (2000) 333.
[21] W. Ueda, K. Oshihara, Appl. Catal., A 200 (2000) 135.
[22] Z. Wang, W. Wie, G. Liu, G. Mao, D. Kuang, Acta Petrol. Sinica 14 (1998) 21.
[23] Y. Han, H. Wang, H. Cheng, J. Deng, Chem. Commun. (1999) 521.
[24] G. Landi, L. Lisi, J.-C. Volta, Catal. Today 91–92C (2004) 275.
[25] E.M. O'Keeffe, F.C. Meunier, J.R.H. Ross, Proceedings of 12° ICC, Granada, 2000.
[26] C.J. Kiely, A. Burrows, S. Sajip, G.J. Hutchings, M.T. Sananes, A. Tuel, J.C. Volta, J. Catal. 162 (1996) 31.
[27] Y. Kamiya, E. Nishikawa, T. Okuhara, T. Hattori, Appl. Catal., A 206 (2001) 103.
[28] A.M. Duarte de Farias, W. de, A. Gonzales, P.G. Pries de Oliveira, J.-G. Eon, J.-M. Herrmann, M. Aouine, S. Loridant, J.-C. Volta, J. Catal. 208 (2002) 238.
[29] M. Abon, K.E. Bere, A. Tuel, P. Delichere, J. Catal. 156 (1995) 28.
[30] Y. Zhang, R.P.A. Sneeden, J.C. Volta, Catal. Today 16 (1993) 39.
[31] F.J. Cabello, R.P.K. Wells, C. Rhodes, G.J. Hutchings, Proceedings of 12° ICC, Granada, 2000.
[32] K. Aït-Lachgar, A. Tuel, M. Brun, J.M. Herrmann, J.M. Krafft, J.R. Martin, J.C. Volta, M. Abon, J. Catal. 177 (1998) 224.
[33] Y. Schuurman, J.T. Gleaves, Catal. Today 33 (1997) 25.
[34] U. Rodemerck, B. Kubias, H.-W. Zanthoff, G.-U. Wolf, M. Baerns, Appl. Catal., A 153 (1997) 217.
[35] S. Albonetti, F. Cavani, F. Trifirò, P. Venturoli, G. Calestani, M. Lopez Granados, J.L.G. Fierro, J. Catal. 160 (1996) 52.
[36] C. Carrara, S. Irusta, E. Lombardo, L. Cornaglia, Appl. Catal., A 217 (2001) 275.
[37] F. Cavani, S. Ligi, T. Monti, F. Pierelli, F. Trifirò, S. Albonetti, G. Mazzoni, Catal. Today 61 (2000) 203.
[38] H.W. Zanthoff, M. Sananes-Schultz, S.A. Buchholz, U. Rodemerck, B. Kubias, M. Baerns, Appl. Catal., A 172 (1998) 49.
[39] A. Matsuura, Catal. Today 16 (1993) 123.
[40] G. Centi, G. Golinelli, F. Trifirò, Appl. Catal. 48 (1989) 13.
[41] L.M. Cornaglia, E.A. Lombardo, J.A. Anderson, J.L. Garcia Fierro, Appl. Catal., A 100 (1993) 37.
[42] A. Tuel, M.T. Sananes-Schulz, J.C. Volta, Catal. Today 37 (1997) 59.
[43] Z.-Y. Xue, G.L. Schrader, J. Phys. Chem. B 103 (1999) 9459.